

On neural and dimensional collapse in supervised and unsupervised contrastive learning with hard negative sampling

Ruijie Jiang^{1†}, Thuan Nguyen^{2†}, Shuchin Aeron¹, Prakash Ishwar^{3*}

November 10, 2023

Abstract

For a widely-studied data model and general loss and sample-hardening functions we prove that the Supervised Contrastive Learning (SCL), Hard-SCL (HSCL), and Unsupervised Contrastive Learning (UCL) risks are minimized by representations that exhibit Neural Collapse (NC), i.e., the class means form an Equiangular Tight Frame (ETF) and data from the same class are mapped to the same representation. We also prove that for any representation mapping, the HSCL and Hard-UCL (HUCL) risks are lower bounded by the corresponding SCL and UCL risks. Although the optimality of ETF is known for SCL, albeit only for InfoNCE loss, its optimality for HSCL and UCL under general loss and hardening functions is novel. Moreover, our proofs are much simpler, compact, and transparent. We empirically demonstrate, for the first time, that ADAM optimization of HSCL and HUCL risks with random initialization and suitable hardness levels can indeed converge to the NC geometry if we incorporate unit-ball or unit-sphere feature normalization. Without incorporating hard negatives or feature normalization, however, the representations learned via ADAM suffer from dimensional collapse (DC) and fail to attain the NC geometry.

1 Introduction

Contrastive representation learning (CL) methods learn a mapping that embeds data into a Euclidean space such that *similar* examples retain close proximity to each other and *dissimilar* examples are pushed apart. CL and in particular unsupervised CL has gained prominence in the last decade with notable success in Natural Language Processing (NLP), Computer Vision (CV), time-series, and other modalities. Recent surveys Balestrieri et al. (2023); Rethmeier and Augenstein (2023) and the references therein provide a comprehensive view of these applications.

Whether or not the learned representation is useful for a downstream classification task depends on the joint distribution of similar and dissimilar data points and how accurately it captures the learning task. In unsupervised (or self-supervised) contrastive learning (UCL) Oh Song et al. (2016); Oord et al. (2018); Wu et al. (2018); Chen et al. (2020); Robinson et al. (2021), similar examples that also referred to as positive examples, are typically constructed via data augmentations or pretext-tasks utilizing domain-specific knowledge of label-invariant augmentations, while dissimilar examples that are also referred to as negative examples, are typically constructed via randomized pairings. In supervised contrastive learning (SCL), full label information is utilized for generating positive and negative examples Khosla et al. (2020).

The focus of this paper is to understand the role of hard-negative sampling in UCL and SCL settings, which when carefully designed has shown to improve downstream classification performance of representations learned

*1 - Tufts University, Dept. of ECE, ² - Tufts University, Dept. of CS, ² - Boston University, Dept. of ECE. † Equal contribution.

via CL Robinson et al. (2020); Jiang et al. (2022, 2023); Long et al. (2023). This paper also studies the impact of feature normalization on the learned representation geometry. In this direction we make the following main contributions.

Main Contributions: Our *main theoretical contributions* are Theorems 1, 2, and 3, which, under a widely-studied latent data model hold for any convex, argument-wise non-decreasing contrastive loss, any non-negative and argument-wise non-decreasing hardening function to generate hard-negative samples, and norm-bounded representations of dimension at least $C - 1$. Theorem 1 establishes that the HSCL loss dominates the SCL loss and similarly the HUCL loss dominates the UCL loss.¹

Theorem 2 is a novel result which states that the globally optimal representation geometry for both SCL and HSCL corresponds to Neural Collapse (NC) (see Definition 7) with the same optimal loss value. Similarly, Theorem 3 establishes the optimality of NC geometry for UCL if the representation dimension is sufficiently large compared to the number of latent classes, which in turn is implicitly determined by the joint distribution of the positive examples that corresponds to the augmentation mechanism.

Our *main empirical contributions* detailed in section 5 show that when using the ADAM optimizer with random initialization, the matrix of class means for SCL is badly conditioned and effectively low-rank, i.e., it exhibits Dimensional Collapse (DC). In contrast, the use of hard negatives at appropriate hardness levels mitigates DC and enables convergence to the global optima. A similar phenomenon is observed for UCL vs HUCL. We also show that feature normalization is also critical for mitigating DC in these settings.

2 Related work

SCL: Theorem 2 in Graf et al. (2021) proves NC for SCL with *empirical* InfoNCE loss relying on delicate combinatorial arguments. In contrast, our Theorem 2 applies to more general CL loss functions, including popular empirical losses, with the proof employing a much simpler sequence of inequalities and probabilistic arguments. As a result, in Theorem 2 *we prove, for the first time, that NC is the optimal geometry for Hard-SCL (HSCL).*

Unlike recent work that show that the *optimization landscape* of supervised learning with least-squares loss is benign Zhou et al. (2022)², in Section 5 we demonstrate that the optimization landscape of SCL is more complicated in that not only is it that the global optimum may not be reached by SGD-like methods with random initialization, the local optima exhibit the dimensional collapse (DC) phenomenon. However, our experiments demonstrate that these issues are remedied via HSCL whose global optimization landscape may be better. Here we note that Yaras et al. (2022) show that with unit-sphere normalization, Riemannian gradient descent methods can achieve the global optima for SCL, underscoring the importance of optimization methods and constraints for training for CL.

UCL: Wang and Isola (2020) argues that asymptotically (in number of negative samples) the InfoNCE loss for UCL, optimizes for a trade-off between alignment of positive pairs while ensuring uniformity of features on the hypersphere. However, a non-asymptotic and global analysis of the optimal solution is still lacking. In contrast, *for UCL in Theorem 3, we show that as long as the embedding dimension is larger than the number of latent classes, which in turn is determined by the distribution of the similar examples, the optimal solution for UCL corresponds to the NC geometry.* In this context, our results complement several recent papers Parulekar et al. (2023); Wen and Li (2021) that study the role of augmentations in UCL.

¹Theorem 3.1 in Wu et al. (2020) is a somewhat similar result for UCL for a special loss function. It does not address hard negatives.

²All critical points other than the global optima are strict saddle points.

We demonstrate that a recent result, viz., Theorem 4 in Jing et al. (2021), that attempts to explain DC in UCL is limited in that under a suitable initialization, the UCL loss trained with ADAM does not exhibit DC (see Section 5). Furthermore, ***we demonstrate for the first time that HUCL mitigates DC in UCL at moderate hardness.*** For CL (without hard-negative sampling), Ziyin et al. (2022) characterize local solutions that correspond to DC but leave open the analysis of training dynamics leading to collapsed solutions.

A geometrical analysis of HUCL is carried out in Robinson et al. (2020), but the optimal solutions are only characterized asymptotically (in the number of negative samples) and for the case when hardness also goes to infinity the analysis seems to require knowledge of supports of class conditional distributions. In contrast, we show that this statement needs revision the geometry of the optimal solution for HUCL depends on the hardness level and in general different compared to UCL due to the possibility of class collision.

3 Contrastive Learning Framework

3.1 Mathematical Set-up and Preliminaries

Notation: $k, C \in \mathbb{N}, C > 1, \mathcal{Y} := \{1, \dots, C\}, \mathcal{Z} \subseteq \mathbb{R}^{dz}$. For $i, j \in \mathbb{Z}, i < j, i : j := i, i + 1, \dots, j$, and $a_{i:j} := a_i, a_{i+1}, \dots, a_j$. If $i > j, i : j$ and $a_{i:j}$ are “null”.

Let $f : \mathcal{X} \rightarrow \mathcal{Z}$ denote a representation mapping from data space \mathcal{X} to representation space $\mathcal{Z} \subseteq \mathbb{R}^{dz}$. Let \mathcal{F} denote a family of such representation mappings.

Contrastive Learning selects a representation from the family by minimizing an expected loss function that penalizes “misalignment” between the representation of an *anchor* sample $z = f(x)$ and the representation of a *positive* sample $z^+ = f(x^+)$ and simultaneously penalizes “alignment” between z and the representations of k *negative* samples $z_i^- := f(x_i^-), i = 1 : k$.

In our work we consider a CL loss function ℓ_{CL} of the following general form.

Definition 1 (Generalized Contrastive Loss).

$$\ell_{CL}(z, z^+, z_{1:k}^-) := \psi(z^\top(z_1^- - z^+), \dots, z^\top(z_k^- - z^+)) \quad (1)$$

where $\psi : \mathbb{R}^k \rightarrow \mathbb{R}$ is a convex function that is also argument-wise non-decreasing (i.e., non-decreasing with respect to each argument when the other arguments are held fixed) throughout \mathbb{R}^k .

This loss subsumes and generalizes popular CL loss functions such as InfoNCE and triplet-loss with sphere-normalized representations. InfoNCE corresponds to $\psi(t_{1:k}) = \log(\alpha + \sum_{i=1}^k e^{t_i})$ for $\alpha > 0^3$ and $\psi(t) = \max\{t + \alpha, 0\}$, $\alpha > 0$ is the triplet-loss with sphere-normalized representations. However, some CL losses such as the spectral contrastive loss of HaoChen et al. (2021) are not of this form.

The CL risk is the expected value of the CL loss:

$$L_{CL}(f) := \mathbb{E}_{(z, z^+, z_{1:k}^-) \sim p_{CL}}[\ell_{CL}(z, z^+, z_{1:k}^-)] \quad (2)$$

where

$$p_{CL}(z, z^+, z_{1:k}^-) = p(z, z^+) \cdot p^-(z_{1:k}^- | z, z^+). \quad (3)$$

Here, the joint probability distribution $p(z, z^+)$ is determined by the underlying joint probability distribution of the anchor and positive samples (x, x^+) and the representation mapping f . If augmentations are used to generate positives, then $p(z, z^+)$ would be determined by the properties of the augmentation mechanism. The

³This is the log-sum-exponential function which is convex over \mathbb{R}^k for all $\alpha \geq 0$ and strictly convex over \mathbb{R}^k if $\alpha > 0$.

conditional probability distribution p^- is designed differently within the unsupervised and supervised settings as described below.

Unsupervised CL (UCL): Here,

$$p^-(z_{1:k}^-|z, z^+) = \prod_{i=1}^k q(z_i^-) \quad (4)$$

where $q(\cdot)$ is a negative-sampling distribution. Thus in UCL, the k negative samples are IID and independent of the anchor and positive sample in the representation space:

$$z_{1:k}^- \sim \text{IID } q \text{ and are independent of } (z, z^+). \quad (5)$$

In the typical unsupervised setting, the anchor and the positive samples have a common marginal probability distribution. In that case, q is taken to be the marginal probability distribution of z (or z^+).

We denote the joint probability distribution of $(z, z^+, z_{1:k}^-)$ in the unsupervised setting by p_{UCL} and the corresponding CL risk by $L_{UCL}(f)$.

Supervised CL (SCL): Here, x, x^+, z, z^+ have a common class label $y \in \mathcal{Y}$ with a class marginal probability distribution $p(y) = \lambda_y \in (0, 1)$ for all $y \in \mathcal{Y}$ and

$$p^-(z_{1:k}^-|z, z^+) = \sum_{y \in \mathcal{Y}} \lambda_y \cdot p_{SCL}^-(z_{1:k}^-|z, z^+, y),$$

where

$$p_{SCL}^-(z_{1:k}^-|z, z^+, y) = \prod_{i=1}^k r(z_i^-|y), \quad (6)$$

$$r(z^-|y) = \sum_{y^- \in \mathcal{Y} \setminus \{y\}} \frac{\lambda_{y^-}}{1 - \lambda_y} s(z^-|y^-), \quad (7)$$

and $s(z^-|y^-)$ is the conditional probability distribution of negative samples in representation space given class y^- . Given z, z^+ and their common class label y , the sampling of z_i^- for each i can be interpreted as first sampling a class label y_i^- **different** from y in a manner consistent with the class marginal probability distribution and then sampling z_i^- from the conditional probability distribution of negative samples in representation space given class y_i^- .

Thus in SCL, the k negative samples are conditionally IID and independent of the anchor and positive sample in the representation space given the anchor label:

$$z_{1:k}^- | y \sim \text{IID } r \text{ and are independent of } (z, z^+). \quad (8)$$

In the typical supervised setting, the anchor and the positive samples have a common conditional probability distribution within each class. In that case $s(\cdot|j)$ is taken to be the conditional probability distribution of z (or z^+) given $y = j$.

We denote the joint probability distribution of $(z, z^+, z_{1:k}^-)$ in the supervised setting by p_{SCL} and the corresponding CL risk by $L_{SCL}(f)$.

For future reference we note that for all $y \in \mathcal{Y}$,

$$\mathbb{E}_{z^- \sim r(z^-|y)}[z^-] = \sum_{j \in \mathcal{Y} \setminus \{y\}} \frac{\lambda_j}{1 - \lambda_y} \mu_j \quad (9)$$

where for all $j \in \mathcal{Y}$,

$$\mu_j := \mathbb{E}_{z^- \sim s(z^-|j)}[z^-]. \quad (10)$$

3.2 CL with Hard Negative Sampling

Hard negative sampling aims to generate negative samples whose representations are “more aligned” with that of the anchor (making them harder to distinguish from the anchor) compared to a given reference negative sampling distribution (whether unsupervised or supervised). We consider a very general class of “hardening” mechanisms that include these classical approaches as special cases. To this end we define a **hardening function** as follows.

Definition 2 (Hardening function). $\eta : \mathbb{R}^k \rightarrow \mathbb{R}$ is a hardening function if it is non-negative and argument-wise non-decreasing throughout \mathbb{R}^k .

As an example, $\eta(t_{1:k}) := \prod_{i=1}^k e^{\beta t_i}$, $\beta > 0$ is an exponential tilting hardening function employed in Robinson et al. (2021); Jiang et al. (2023).

Hard UCL (HUCL): Let $p_{UCL}^-(z_{1:k}^- | z, z^+) := \prod_{i=1}^k q(z_i^-)$ be a reference negative sampling probability distribution for UCL and η a hardening function such that for all $z \in \mathcal{Z}$,

$$\gamma(z) := \mathbb{E}_{z_{1:k}^- \sim \text{IID } q}[\eta(z^\top z_1^-, \dots, z^\top z_k^-)] \in (0, \infty). \quad (11)$$

We define the η -harder negative sampling probability distribution for UCL as follows.

Definition 3 (η -harder negatives for UCL).

$$p_{HUCL}^-(z_{1:k}^- | z, z^+) := \frac{\eta(z^\top z_1^-, \dots, z^\top z_k^-)}{\gamma(z)} \cdot \prod_{i=1}^k q(z_i^-). \quad (12)$$

We observe that negative samples which are more aligned with the anchor in representation space, i.e., when $z^\top z_i^-$ is large, are sampled relatively more often in p_{HUCL}^- than in the reference p_{UCL}^- because η is argument-wise non-decreasing throughout \mathbb{R}^k .

We note that in HUCL, $z_{1:k}^-$ are conditionally independent of z^+ given z , but they are not independent of z (unlike in UCL). Moreover, $z_{1:k}^-$ may not be conditionally IID given z if the hardening function is not (multiplicatively) separable.

We denote the joint probability distribution of $(z, z^+, z_{1:k}^-)$ in the hard UCL setting by p_{HUCL} and the corresponding CL risk by $L_{HUCL}(f)$.

Hard SCL (HSCL): Let $p_{SCL}^-(z_{1:k}^- | z, z^+, y) = \prod_{i=1}^k r(z_i^- | y)$ be a reference class-conditional negative sampling probability distribution for SCL and η a hardening function such that for all $y \in \mathcal{Y}$ and all $z \in \mathcal{Z}$,

$$\gamma(z, y) := \mathbb{E}_{z_{1:k}^- \sim \text{IID } r(\cdot | y)}[\eta(z^\top z_1^-, \dots, z^\top z_k^-)] \in (0, \infty).$$

We define the η -harder class-conditional negative sampling probability distribution for SCL as follows.

Definition 4 (η -harder negatives for SCL).

$$p_{HSCL}^-(z_{1:k}^- | z, z^+, y) := \frac{\eta(z^\top z_1^-, \dots, z^\top z_k^-)}{\gamma(z, y)} \prod_{i=1}^k r(z_i^- | y). \quad (13)$$

We note that in HSCL, $z_{1:k}^-$ are conditionally independent of z^+ given y and z but they are not conditionally independent of z given y (unlike in SCL). Moreover, $z_{1:k}^-$ may not be conditionally IID given (y, z) if the hardening function is not separable.

We denote the joint probability distribution of $(z, z^+, z_{1:k}^-)$ in the hard SCL setting by p_{HSCL} and the corresponding CL risk by $L_{HSCL}(f)$.

4 Theoretical Results

In this section we present our main theoretical results using the notation and mathematical framework for CL described in the previous section. Due to space constraints, we only present the detailed proof of Theorem 2 here. Detailed proofs of the remaining results are provided in Appendix A.

Theorem 1 (Hard CL versus CL). *Let ψ in (1) be argument-wise non-decreasing over \mathbb{R}^k and assume that all expectations associated with $L_{UCL}(f), L_{HUCL}(f), L_{SCL}(f), L_{HSCL}(f)$ exist and are finite. Then, for all f , $L_{HUCL}(f) \geq L_{UCL}(f)$ and $L_{HSCL}(f) \geq L_{SCL}(f)$.*

We note that convexity of ψ is not needed in Theorem 1. The proof of Theorem 1 is based on the generalized association inequality due to Harris, Theorem 2.15 Boucheron et al. (2013), and is presented in Appendix A.

Lower Bound for SCL and “Neural Collapse”: Consider the supervised setting in which the anchor and the positive samples are conditionally IID given their common label y . In (7), let $s(\cdot|y)$ be the conditional probability distribution of z (or equivalently z^+) given y . Thus, $p(z, z^+|y) = s(z|y) \cdot s(z^+|y)$. Suppose that the representation space is confined to the unit closed ball in Euclidean space and that the marginal probability distribution of the class label of the anchor (or equivalently the positive sample) is uniform. Then for all $y \in \mathcal{Y}$, $\lambda_y = \frac{1}{C}$ and given y ,

$$\mathbb{E}_{z \sim p(z|y)}[z] = \mathbb{E}_{z^+ \sim p(z^+|y)}[z^+] = \mathbb{E}_{z^- \sim s(z^-|y)}[z^-] = \mu_y$$

i.e., under the modeling assumptions stated above, the anchor, positive, and negative samples all have the same class-conditional means and

$$\mathbb{E}_{z^- \sim r(z^-|y)}[z^-] = \frac{1}{C-1} \sum_{i \in \mathcal{Y} \setminus \{y\}} \mu_i$$

where $r(\cdot|y)$ is as in (7). Moreover, for all $i = 1 : k$,

$$\begin{aligned} \mathbb{E}[z^\top z_i^-] &= \sum_{y \in \mathcal{Y}} \frac{1}{C} \sum_{y_i^- \in \mathcal{Y} \setminus \{y\}} \frac{1}{C-1} \mathbb{E}_{z \sim s(\cdot|y)}[z^\top] \cdot \mathbb{E}_{z_i^- \sim s(\cdot|y_i^-)}[z_i^-] \\ &= \frac{1}{C(C-1)} \sum_{j, \ell \in \mathcal{Y}, j \neq \ell} \mu_j^\top \mu_\ell. \end{aligned} \quad (14)$$

Within this setting we have the following lower bound for the SCL risk and conditions for equality.

Theorem 2 (Lower bound for SCL risk with norm-bounded representations and equiprobable classes). *Let $\mathcal{Z} = \{z \in \mathbb{R}^{d_z} : \|z\| \leq 1\}$. For all $y \in \mathcal{Y}$, let $\lambda_y = \frac{1}{C}$ and $z, z^+|y \sim \text{IID } s(\cdot|y)$, where $s(\cdot|y)$ is the same as in (7).*

For all $y \in \mathcal{Y}$, let $\mu_y := \mathbb{E}_{z \sim s(\cdot|y)}[z]$. Let ψ be a convex function that is also argument-wise non-decreasing throughout \mathbb{R}^k . Then for all $f : \mathcal{X} \rightarrow \mathcal{Z}$,

$$L_{SCL}(f) \geq \psi \left(\frac{-C}{(C-1)}, \dots, \frac{-C}{(C-1)} \right). \quad (15)$$

If ψ is a strictly convex function that is also argument-wise strictly increasing throughout \mathbb{R}^k , then equality in (15) holds if, and only if, $\forall j, \ell \in \mathcal{Y} : j \neq \ell$,

$$\mu_j^\top \mu_\ell = \frac{-1}{C-1} \text{ (equal angle class means),}$$

Then,

1. $\sum_{j \in \mathcal{Y}} \mu_j = 0$ (zero sum of class means),

2. $\forall j \in \mathcal{Y}, \|\mu_j\| = 1$ (unit-norm class means),

3. $L_{HSCL}(f) = L_{SCL}(f)$.

Definition 5 (ETF). *The equal angle, zero sum, and unit-norm conditions on class means in Theorem 2 define a (normalized) Equiangular Tight Frame (ETF) Malozemov and Pevnyi (2009). The matrix $M := [\mu_1, \dots, \mu_C] \in \mathbb{R}^{d_Z \times C}$ has $C - 1$ nonzero singular values all equal to $\sqrt{\frac{C}{C-1}}$ and rank equal to $C - 1 \leq d_Z$.*

Definition 6 (Variance Collapse for CL). *We will say representation map $f(\cdot)$ attains Variance Collapse for CL if for all $j \in \mathcal{Y}$, $\Pr(z = \mu_j | y = j) = 1$, i.e., the representations of all samples in each class collapse to their common class mean vector.*

Definition 7 (Neural Collapse (NC) for CL). *We will say representation map $f(\cdot)$ attains Neural Collapse for CL if it attains Variance Collapse for CL as in Definition 6 and the class means in representation space form a normalized ETF as in Definition 5.*

Corollary 1. *The unit-norm class means condition in Theorem 2 implies Variance Collapse for CL. Consequently, the lower bound in Theorem 2 can be attained if, and only if, we have Neural Collapse for CL.*

Proof. Jensen’s inequality for the strictly convex function $\|\cdot\|^2$ together with $\|z\|^2 \leq 1$ with probability one imply that $1 \geq \mathbb{E}_{z \sim p(z|y)}[\|z\|^2] \geq \|\mathbb{E}_{z \sim p(z|y)}[z]\|^2 = \|\mu_y\|^2 = 1$. This implies that we have equality in Jensen’s inequality, which can occur iff with probability one given y , we have $z = \mu_y$. \square

Remark 1 (Attaining the SCL lower bound). *The strict convexity and strictly increasing conditions on ψ in Theorem 2 ensure that the lower bound can be attained only if the representation map f attains Neural Collapse for CL. Theorem 2 also holds for **empirical risk** because empirical risk can be expressed as an expectation with a uniform distribution over the dataset. If the family of representation mappings \mathcal{F} has sufficiently high capacity⁴ and $\forall y \in \mathcal{Y}$, $p(x|y), p(x^+|y), p(x_i^-|y)$, $i = 1 : k$, are all discrete probability mass functions (pmfs) over finite sets⁵ with support-sets that are disjoint across different classes, then the equal angle condition in Theorem 2 can be satisfied for a suitable f in the family. If either convexity or monotonicity of ψ is not strict, e.g., $\psi(t) = \max\{t + \alpha, 0\}$, then it may be possible for a representation map f to attain the lower bound without attaining Neural Collapse for CL.*

Proof. The zero-sum and unit-norm conditions follow from the equal angle and unit-ball representation conditions by a short computation (see Appendix A.2).

We have $(z, z^+, z_{1:k}^-) \sim p_{SCL}$ and

$$\begin{aligned} L_{SCL} &= \mathbb{E}_{z, z^+, z_{1:k}^-} [\psi(z^\top(z_1^- - z^+), \dots, z^\top(z_k^- - z^+))] \\ &\geq \mathbb{E}_{z, z^+, z_{1:k}^-} [\psi(z^\top z_1^- - 1, \dots, z^\top z_k^- - 1)] \end{aligned} \tag{16}$$

$$\geq \psi(\mathbb{E}_{z, z_1^-} [z^\top z_1^-] - 1, \dots, \mathbb{E}_{z, z_k^-} [z^\top z_k^-] - 1) \tag{17}$$

$$\geq \psi\left(\frac{-C}{(C-1)}, \dots, \frac{-C}{(C-1)}\right) \tag{18}$$

which is the lower bound in (15). Inequality (16) is true because ψ is argument-wise non-decreasing and $z^\top z^+ \leq 1$ since $\|z\|, \|z^+\| \leq 1$. Inequality (17) is Jensen’s inequality applied to the convex function ψ .

⁴For example, all mappings implemented by a sufficiently deep and wide neural network.

⁵For example, uniform pmfs over a finite sequence of training samples within each class.

Finally, inequality (18) follows from (14) and the following analysis together with the fact that ψ is an argument-wise non-decreasing function:

$$\begin{aligned}
\forall i, \quad \mathbb{E}[z^\top z_i^-] &= \frac{1}{C(C-1)} \sum_{j, \ell \in \mathcal{Y}, j \neq \ell} \mu_j^\top \mu_\ell \\
&= \frac{1}{C(C-1)} \left(\left\| \sum_{j \in \mathcal{Y}} \mu_j \right\|^2 - \sum_{j \in \mathcal{Y}} \|\mu_j\|^2 \right) \\
&\geq \frac{1}{C(C-1)}(0 - C) = \frac{-1}{C-1}
\end{aligned} \tag{19}$$

where inequality (19) holds because $\|\cdot\|^2 \geq 0$ and for all $j \in \mathcal{Y}$, $\|\mu_j\| \leq 1$.

The lower bound in (15) can be attained iff we have equality in (19), (18), (17), and (16). Equality in (19) holds iff for all $j \in \mathcal{Y}$, $\|\mu_j\| = 1$ (the unit-norm class means condition in Theorem 2) and $\sum_{j \in \mathcal{Y}} \mu_j = 0$ (the zero sum of class means condition in Theorem 2). If ψ is argument-wise *strictly* increasing, then equality in (18) holds iff equality holds in (19).

Equality in (17) holds iff we have equality in Jensen's inequality which, if ψ is *strictly* convex, can occur iff for all $i \in [1 : k]$, $\Pr(z^\top z_i^- = \beta_i) = 1$ for some constant β_i . Equality in (17), (18), and (19) can occur jointly iff $\forall i \in [1 : k], \beta_i = \beta$ for some constant β .

Equality in (16) holds if it holds in (19) because equality in (19) implies the unit-norm condition which (per Corollary 1) implies that $\forall j \in \mathcal{Y}$, $\Pr(z = \mu_j | y = j) = 1$. Then, $z^\top z^+ = 1$ with probability one because (z, z^+) are conditionally IID given y and all labels have a strictly positive probability.

With equality in (19), (18), (17), and (16), $\forall i = 1 : k$, $\Pr(z^\top z_i^- = \beta) = 1 \Rightarrow$ for each i and all $j, \ell \in \mathcal{Y}$, with $j \neq \ell$, we will have $\Pr(z^\top z_i^- = \beta | y = j, y_i^- = \ell) = 1$ because all pairs of *distinct* label values for y and y_i^- have a strictly positive probability. For all $j \in \mathcal{Y}$, $\Pr(z = \mu_j | y = j) = 1$ and also for all $\ell \in \mathcal{Y}$, $\Pr(z_i^- = \mu_\ell | y = \ell) = 1$ (negatives have the same class-conditional distribution as the anchor). Then for all $j, \ell \in \mathcal{Y}$, with $j \neq \ell$, we will have $\mu_j^\top \mu_\ell = \beta$ which is the equal angle class means condition in Theorem 2.

To summarize, if ψ is *strictly* convex and is argument-wise *strictly* increasing throughout \mathbb{R}^k , then the lower bound in Theorem 2 can be attained iff equality holds in (19), (18), (17), (16) \Leftrightarrow

For all $j \in \mathcal{Y}$, $\|\mu_j\| = 1$, $\sum_{j \in \mathcal{Y}} \mu_j = 0$, and for all $i \in [1 : k]$, $\Pr(z^\top z_i^- = \beta) = 1$ for some constant $\beta \Leftrightarrow$ For all $j \in \mathcal{Y}$, $\|\mu_j\| = 1$, $\sum_{j \in \mathcal{Y}} \mu_j = 0$, and for all $\forall j, \ell \in \mathcal{Y} : j \neq \ell$, $\mu_j^\top \mu_\ell = \beta$. Under these conditions, we must have $\beta = \frac{-1}{C-1}$ since $0 = \left\| \sum_{j \in \mathcal{Y}} \mu_j \right\|^2 = \sum_{j, \ell \in \mathcal{Y}, j \neq \ell} \mu_j^\top \mu_\ell - \sum_{j \in \mathcal{Y}} \|\mu_j\|^2 = C(C-1)\beta - C \times 1$.

Moreover, under these conditions, with probability one $z^\top z_i^- = \beta$ simultaneously for all $i = 1 : k$ and $\eta(z^\top z_1^-, \dots, z^\top z_k^-) = \eta(\beta, \dots, \beta)$, a constant. Consequently, for all z, y we must have $\gamma(z, y) = \eta(\beta, \dots, \beta)$ which would imply that (see Equation 13) $p_{HSCL} = p_{SCL}$ and $L_{HSCL}(f) = L_{SCL}(f)$. \square

Lower Bound for UCL with latent structure and “Neural Collapse”: Consider the unsupervised setting in which $p(z, z^+) = \frac{1}{C} \sum_{y=1}^C s(z|y)s(z^+|y)$ and $q(z^-) = \frac{1}{C} \sum_{y=1}^C s(z^-|y^-)$. Here y is to be interpreted as a *latent class or cluster* and $s(\cdot|y)$ as the conditional distribution, in representation space, of samples within latent class y . The anchor, positive, and negative samples all have the same marginal distribution $q(\cdot)$. This latent model is consistent with the setting where the anchor and positive samples are generated via IID randomized augmentations from a reference sample and a negative sample is generated in the same way but from an independently generated reference sample.

Theorem 3 (Lower bound for UCL risk with latent structure, norm-bounded representations, and equiprobable classes). *Let $\mathcal{Z} = \{z \in \mathbb{R}^{d_z} : \|z\| \leq 1\}$, $p(z, z^+) = \frac{1}{C} \sum_{y \in \mathcal{Y}} s(z|y)s(z^+|y)$, and $q(z^-) = \frac{1}{C} \sum_{y \in \mathcal{Y}} s(z^-|y^-)$, where $s(\cdot|j)$ is a conditional probability distribution of samples in representation space given latent class j .*

Let ψ be a convex function that is also argument-wise non-decreasing throughout \mathbb{R}^k . Then for all $f : \mathcal{X} \rightarrow \mathcal{Z}$,

$$L_{UCL}(f) \geq \frac{1}{C^{k+1}} \sum_{y, y_{1:k} \in \mathcal{Y}} \psi \left(\frac{-C1(y_1^- \neq y)}{C-1}, \dots, \frac{-C1(y_k^- \neq y)}{C-1} \right) \quad (20)$$

where $1(\cdot)$ is the indicator function.

If ψ is a strictly convex function that is also argument-wise strictly increasing throughout \mathbb{R}^k , then equality in (20) holds if, and only if, the equal angle condition of Theorem 2 holds for the latent class means. Then, the zero sum and unit-norm conditions of Theorem 2 will also hold for the latent class means.

Similarly to Corollary 1 and Remark 1, the lower bound for $L_{UCL}(f)$ can be attained iff we have Neural Collapse (for UCL). But **unlike in Theorem 2, here we cannot assert that if the lower bound is attained, then we will have $L_{HUCL}(f) = L_{UCL}(f)$** . This is because in the UCL and HUCL settings, the negative sample can come from the same latent class as the anchor (latent class collision) with a positive probability ($\frac{1}{C^2}$). Then under Neural Collapse, we cannot conclude that with probability one $\eta(z^\top z_1^-, \dots, z^\top z_k^-) = \eta(\beta, \dots, \beta)$, for some constant β . **Deriving a tight lower bound for HUCL and determining whether it can be attained iff there is Neural Collapse for UCL are open problems.** Neural Collapse in SCL or UCL requires that the representation space dimension $d_{\mathcal{Z}} \geq C - 1$. This can be ensured in SCL since labels are available and the number of classes is known. In UCL the number of latent classes is not known and is only implicitly specified by the sample generating mechanism. Thus **even if it was possible to attain the global minimum of the empirical UCL loss, neural collapse may not be observed unless $d_{\mathcal{Z}}$ is chosen to be sufficiently large.**

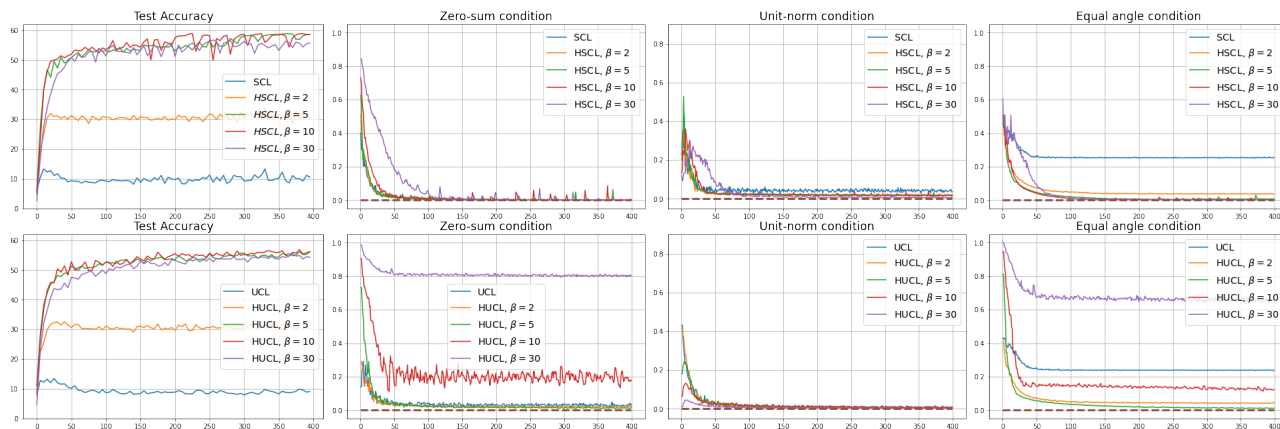


Figure 1: Results for CIFAR100 under supervised settings (SCL, HSCL, top row) and unsupervised settings (UCL, HUCL, bottom row) with unit-ball normalization and random initialization. From left to right: Downstream Test Accuracy, Zero-sum metric, Unit-norm metric, and Equal angle metric *vs.* number of Epochs.

5 Practical achievability of global optima for CL

In this section, we investigate the achievability of global optima for UCL, SCL, HUCL, and HSCL using two image datasets: CIFAR10 and CIFAR100 Krizhevsky et al. (2009). Both datasets comprise of $32 \times 32 \times 3$ images with 10 classes (CIFAR10) or 100 classes (CIFAR100), respectively. We observed very similar phenomena in CIFAR100 and CIFAR10. Due to limited space, we only present results for CIFAR100 here. Results for CIFAR10 are in Appendix B.

We utilize the InfoNCE loss with the exponential form hardening function, as described in Sec. 3.1. To maintain consistency with the proposed theory, for all four CL settings (UCL, SCL, HUCL, and HSCL), for a given anchor z , we randomly sample the positive sample z^+ from the class conditional distribution corresponding to the class of z . Therefore, the only distinction among our four training settings is their negative sampling distribution $p^-(z_{1:k}^-|z, z^+)$.

We utilized the ResNet-50 architecture He et al. (2016) to implement the representation function f . We set the representation dimension to $d = C - 1$, which is the smallest dimension needed to observe Neural Collapse (see Definition 5), and normalize representations to be within a unit ball; further details are provided in Algorithm 1, lines 5-12, in Appendix B. We set the number of negative samples to $k = 256$ (results change negligibly for $k \in [32, 512]$). The hyper-parameter β , which modulates hardness, was chosen from the set $\{0, 2, 5, 10, 30\}$. Each model underwent training for $E = 400$ epochs with a batch size of $B = 512$. We used the ADAM optimizer with learning rate 10^{-3} . All computations were executed on NVIDIA A100 32 GB GPU.

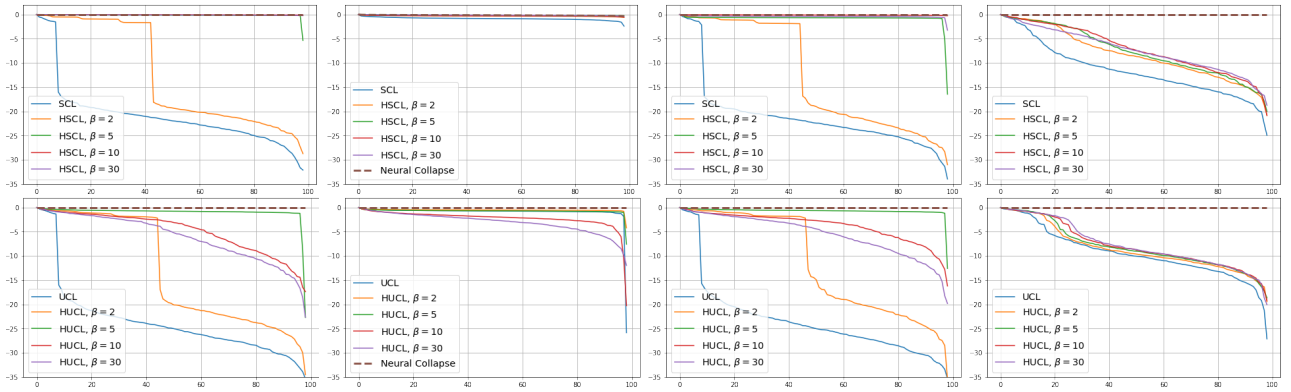


Figure 2: Normalized singular values of empirical covariance matrix of class means (in representation space) plotted in log-scale for CIFAR100 under supervised (top row) and unsupervised (bottom row) settings. From left to right: Unit-ball normalization with random initialization, Unit-ball normalization with NC initialization, Unit-sphere normalization with random initialization, and un-normalized representation with random initialization.

First, we show that **hard negative sampling improves downstream classification performance**. As shown in Fig. 1, first column, we see that with negative sampling at moderate hardness levels ($\beta = 5, 10$), the classification accuracy of HSCL and HUCL is $> 40\%$ points more than that of SCL and UCL.

Achievability of neural collapse:

We test whether the SCL and UCL when trained using ADAM achieve the globally optimal solution corresponding to Neural Collapse (NC). To test this, in line with Theorems 2 and 3, we employ the following metrics, which are plotted in Fig. 1 in the third through fourth columns.

1. **Zero-sum metric:** $\left\| \sum_{j \in \mathcal{Y}} \mu_j \right\|$;
2. **Unit-norm metric:** $\frac{1}{C} \sum_{j \in \mathcal{Y}} \left| \|\mu_j\| - 1 \right|$;
3. **Equal-angle metric:** $\frac{1}{C(C-1)} \sum_{\substack{j, k \in \mathcal{Y}, \\ k \neq j}} \left| \mu_j^\top \mu_k + \frac{1}{C-1} \right|$.

We note that even though the equal angle class means condition together with unit-ball normalization implies the zero-sum and unit-norm conditions, we report these three metrics separately to gain more insight.

According to Theorems 2 and 3, the optimal solutions for UCL, SCL, and HSCL are anticipated to manifest NC. However, our experimental findings reveal a gap between the theoretical expectations and the observed

outcomes. Specifically, both SCL and UCL, when leveraging the regular negative sampling method, do not achieve NC, especially for zero-sum and equal angle class means conditions (columns 2, 4 in Fig. 1). This is also evidenced by Table 1 that shows the theoretically optimal and empirical losses from the experiments. While our theoretical results posit that two training methods SCL and HSCL should induce the same optimal solution, the empirical result of SCL deviates noticeably. On the other hand, increased hardness in HSCL, especially at $\beta = 5, 10$, can bring the loss values close to the theoretical result.

Theory	Empirical				
	SCL	HSCL			
0.3105	$\beta = 0$	$\beta = 2$	$\beta = 5$	$\beta = 10$	$\beta = 30$
	0.3384	0.3603	0.3106	0.3107	0.3222

Table 1: Comparison of theoretical and empirical loss values (after 400 epochs) for CIFAR100.

In addition, the dynamics of the hard negative sampling methods display marked differences in supervised versus unsupervised settings. Specifically, in supervised learning, increased hardness invariably leads to improved results, and the model tends to approach NC, notably at $\beta = 5, 10, 30$. However, in the unsupervised settings, there seems to be just a single optimal hardness level, best observed at $\beta = 5$.

5.1 Dimensional Collapse

To gain further insights, we investigate the phenomenon of Dimensional Collapse (DC) that is known to occur in contrastive learning Jing et al. (2021).

Definition 8. [*Dimension Collapse (DC)*] We say that the class means μ_1, \dots, μ_C suffer from DC if their empirical covariance matrix has one or more singular values that are zero or orders of magnitude smaller than the largest singular value.

If $d_{\mathcal{Z}} = C - 1$ then under neural collapse (NC), the class mean vectors would have full rank $C - 1$ in representation space due to the ETF condition. Thus when $d_{\mathcal{Z}} = C - 1$, $NC \Rightarrow \neg DC$ but we note that $\neg DC \not\Rightarrow NC$, which could occur, for example, if the zero-sum condition in Theorem 2 is not satisfied but the other two are.

We numerically assess DC by plotting the singular values of the empirical covariance matrix of the class means normalized by the largest singular value.

The results of DC for UCL, SCL, HUCL, and HSCL are shown in Fig. 2. In the supervised settings, (top row in Fig. 2), the results align with our previous observations from Fig. 1.

However, in the unsupervised settings (bottom row in Fig. 2), while HUCL with high hardness values deviates more from neural collapse compared to UCL in Fig. 1, in Fig. 2 we see that HUCL suffers less from DC.

Role of initialization: To gain further insights into the results of Fig. 2, we trained a model using HSCL with $\beta = 10$ for 400 epochs until it nearly reaches NC (as measured by the metrics). We then use this pre-trained model as initialization for ADAM for all the other set-ups, viz., UCL, SCL, HUCL, and HSCL. We observe that:

- SCL and HSCL trained with near-NC initialization and ADAM do not exhibit DC.
- UCL trained with near-NC initialization and ADAM also does not exhibit DC, but the behavior of HUCL depends on the hardness level β . This is because at higher β , due to class collisions, the DC phenomenon becomes more pronounced.

Role of normalization: We show that feature normalization plays an important role in alleviating DC. To show this, we test three constraints while training: (1) unit-ball normalization, (2) unit-sphere normalization, and (3) no normalization. The results are shown in Fig. 2. As observed, the behavior of unit-sphere normalization is close to that of unit-ball normalization, and with hard negative sampling, both SCL and UCL can achieve NC.

Without normalization, neither regular nor hard negative training methods attain NC and they suffer from DC. We also observe that with regular negative sampling, no normalization led to less DC for both SCL and UCL. However, hard-negative sampling benefits more from feature normalization and its absence leads to more severe DC.

6 Conclusion and Open Questions

We proved the theoretical optimality of the NC geometry for SCL, UCL, and notably (for the first time) HSCL risks for a very general family of CL losses and hardening functions that subsume popular choices. We empirically demonstrated the ability of hard-negative sampling to achieve global optima for CL and mitigate dimension collapse, in both supervised and unsupervised settings. Our theoretical and empirical results motivate a number of open questions. Firstly, a tight lower bound for HUCL remains open due to latent-class collision. It is also unclear whether the HUCL risk is minimized iff there is Neural Collapse. A difficulty with empirically observing NC in UCL and HUCL is that the number of latent classes is not known because it is, in general, implicitly tied to the properties of the sampling distribution. Thus, in order to observe NC we may need to choose a sufficiently large representation dimension. Another open question is to unravel precisely how and why hard negatives alter the optimization landscape enabling the training dynamics of ADAM with random initialization to converge to the global optimum for suitable hardness levels, and additionally what are optimum choices for hardness levels.

7 Acknowledgements

Ruijie Jiang and Shuchin Aeron would like to acknowledge the support by NSF DRL 1931978.

References

- Balestriero, R., Ibrahim, M., Sobal, V., Morcos, A., Shekhar, S., Goldstein, T., Bordes, F., Bardes, A., Mialon, G., Tian, Y., et al. (2023). A cookbook of self-supervised learning. *arXiv preprint arXiv:2304.12210*.
- Boucheron, S., Lugosi, G., and Massart, P. (2013). *Concentration Inequalities - A Nonasymptotic Theory of Independence*. Oxford University Press.
- Chen, T., Kornblith, S., Norouzi, M., and Hinton, G. (2020). A simple framework for contrastive learning of visual representations. In *International conference on machine learning*, pages 1597–1607. PMLR.
- Graf, F., Hofer, C., Niethammer, M., and Kwitt, R. (2021). Dissecting supervised contrastive learning. In *International Conference on Machine Learning*, pages 3821–3830. PMLR.
- HaoChen, J. Z., Wei, C., Gaidon, A., and Ma, T. (2021). Provable guarantees for self-supervised deep learning with spectral contrastive loss. *Advances in Neural Information Processing Systems*, 34:5000–5011.
- He, K., Zhang, X., Ren, S., and Sun, J. (2016). Deep residual learning for image recognition. In *2016 IEEE Conference on Computer Vision and Pattern Recognition (CVPR)*, pages 770–778.

- Jiang, R., Ishwar, P., and Aeron, S. (2023). Hard negative sampling via regularized optimal transport for contrastive representation learning. In *2023 International Joint Conference on Neural Networks (IJCNN)*, pages 1–8. IEEE.
- Jiang, R., Nguyen, T., Ishwar, P., and Aeron, S. (2022). Supervised contrastive learning with hard negative samples. *arXiv preprint arXiv:2209.00078*.
- Jing, L., Vincent, P., LeCun, Y., and Tian, Y. (2021). Understanding dimensional collapse in contrastive self-supervised learning. In *International Conference on Learning Representations*.
- Khosla, P., Teterwak, P., Wang, C., Sarna, A., Tian, Y., Isola, P., Maschinot, A., Liu, C., and Krishnan, D. (2020). Supervised contrastive learning. *Advances in Neural Information Processing Systems*, 33:18661–18673.
- Krizhevsky, A., Hinton, G., et al. (2009). Learning multiple layers of features from tiny images.
- Long, Z., Killick, G., McCreadie, R., Camarasa, G. A., and Meng, Z. (2023). When hard negative sampling meets supervised contrastive learning.
- Malozemov, V. N. and Pevnyi, A. B. (2009). Equiangular tight frames. *Journal of Mathematical Sciences*, 157(6):789–815.
- Oh Song, H., Xiang, Y., Jegelka, S., and Savarese, S. (2016). Deep metric learning via lifted structured feature embedding. In *Proceedings of the IEEE conference on computer vision and pattern recognition*, pages 4004–4012.
- Oord, A. v. d., Li, Y., and Vinyals, O. (2018). Representation learning with contrastive predictive coding. *arXiv preprint arXiv:1807.03748*.
- Parulekar, A., Collins, L., Shanmugam, K., Mokhtari, A., and Shakkottai, S. (2023). Infonce loss provably learns cluster-preserving representations. *arXiv preprint arXiv:2302.07920*.
- Rethmeier, N. and Augenstein, I. (2023). A primer on contrastive pretraining in language processing: Methods, lessons learned, and perspectives. *ACM Computing Surveys*, 55(10):1–17.
- Robinson, J. D., Chuang, C.-Y., Sra, S., and Jegelka, S. (2020). Contrastive learning with hard negative samples. In *International Conference on Learning Representations*.
- Robinson, J. D., Chuang, C.-Y., Sra, S., and Jegelka, S. (2021). Contrastive learning with hard negative samples. In *International Conference on Learning Representations*.
- Wang, T. and Isola, P. (2020). Understanding contrastive representation learning through alignment and uniformity on the hypersphere. In *International Conference on Machine Learning*, pages 9929–9939. PMLR.
- Wen, Z. and Li, Y. (2021). Toward understanding the feature learning process of self-supervised contrastive learning. In *International Conference on Machine Learning*, pages 11112–11122. PMLR.
- Wu, M., Mosse, M., Zhuang, C., Yamins, D., and Goodman, N. (2020). Conditional negative sampling for contrastive learning of visual representations. *arXiv preprint arXiv:2010.02037*.
- Wu, Z., Xiong, Y., Yu, S. X., and Lin, D. (2018). Unsupervised feature learning via non-parametric instance discrimination. In *Proceedings of the IEEE conference on computer vision and pattern recognition*, pages 3733–3742.

- Yaras, C., Wang, P., Zhu, Z., Balzano, L., and Qu, Q. (2022). Neural collapse with normalized features: A geometric analysis over the riemannian manifold. *Advances in neural information processing systems*, 35:11547–11560.
- Zhou, J., Li, X., Ding, T., You, C., Qu, Q., and Zhu, Z. (2022). On the optimization landscape of neural collapse under mse loss: Global optimality with unconstrained features. In *International Conference on Machine Learning*, pages 27179–27202. PMLR.
- Ziyin, L., Lubana, E. S., Ueda, M., and Tanaka, H. (2022). What shapes the loss landscape of self supervised learning? In *The Eleventh International Conference on Learning Representations*.

A PROOFS

A.1 Proof of Theorem 1

Lemma 1 (Harris Inequality, Theorem 2.15 in Boucheron et al. (2013)). *Let $g : \mathbb{R}^k \rightarrow \mathbb{R}$ and $h : \mathbb{R}^k \rightarrow \mathbb{R}$ be argument-wise non-decreasing throughout \mathbb{R}^k . If $u_{1:k} \sim \text{IID } p$ then*

$$\begin{aligned} \mathbb{E}_{u_{1:k} \sim \text{IID } p}[g(u_{1:k})h(u_{1:k})] &\geq \\ &\mathbb{E}_{u_{1:k} \sim \text{IID } p}[g(u_{1:k})] \cdot \mathbb{E}_{u_{1:k} \sim \text{IID } p}[h(u_{1:k})] \end{aligned}$$

whenever the expectations exist and are finite.

Corollary 2. *Let $\eta : \mathbb{R}^k \rightarrow \mathbb{R}$ be non-negative and argument-wise non-decreasing throughout \mathbb{R}^k such that $\gamma := \mathbb{E}_{u_{1:k} \sim \text{IID } p}[\eta(u_{1:k})] \in (0, \infty)$. Let $p_H(u_{1:k}) := \frac{\eta(u_{1:k})}{\gamma} \prod_{i=1}^k p(u_i)$. If $g : \mathbb{R}^k \rightarrow \mathbb{R}$ is argument-wise non-decreasing throughout \mathbb{R}^k such that $\mathbb{E}_{u_{1:k} \sim \text{IID } p}[g(u_{1:k})]$ exists and is finite, then*

$$\mathbb{E}_{u_{1:k} \sim p_H}[g(u_{1:k})] \geq \mathbb{E}_{u_{1:k} \sim \text{IID } p}[g(u_{1:k})]$$

Proof.

$$\begin{aligned} &\mathbb{E}_{u_{1:k} \sim p_H}[g(u_{1:k})] \\ &= \mathbb{E}_{u_{1:k} \sim \text{IID } p} \left[g(u_{1:k}) \frac{\eta(u_{1:k})}{\gamma} \right] \\ &\geq \mathbb{E}_{u_{1:k} \sim \text{IID } p}[g(u_{1:k})] \frac{\mathbb{E}_{u_{1:k} \sim \text{IID } p}[\eta(u_{1:k})]}{\gamma} \\ &= \mathbb{E}_{u_{1:k} \sim \text{IID } p}[g(u_{1:k})] \end{aligned}$$

where the inequality in the second step follows from the Harris inequality (see Lemma 1). \square

Proof of Theorem 1. The proof essentially follows from Corollary 2 by defining $u_i := z^\top z_i^-$ for $i = 1 : k$, $g_{z,z^+}(u_{1:k}) := \psi(u_1 - z^\top z^+, \dots, u_k - z^\top z^+)$, noting that $u_{1:k}$ are conditionally IID given (z, z^+) in the UCL setting and conditionally IID given (z, z^+, y) in the SCL setting, and verifying that the conditions of Corollary 2 hold.

For clarity, we provide a detailed proof of the inequality $L_{HSCL}(f) \geq L_{SCL}(f)$. The detailed proof of the inequality $L_{HUCL}(f) \geq L_{UCL}(f)$ parallels that for the (more intricate) supervised setting and is omitted.

$$\begin{aligned} L_{HSCL}(f) &= \\ &= \mathbb{E}_{(z,z^+,y) \sim p(z,z^+,y)} \left[\mathbb{E}_{z_{1:k}^- \sim p_{HSCL}^-(z_{1:k}^- | z, z^+, y)} \left[\psi(z^\top(z_1^- - z^+), \dots, z^\top(z_k^- - z^+)) \right] \right] \\ &= \mathbb{E}_{(z,z^+,y) \sim p(z,z^+,y)} \left[\mathbb{E}_{z_{1:k}^- \sim \text{IID } r(\cdot | y)} \left[\psi(z^\top(z_1^- - z^+), \dots, z^\top(z_k^- - z^+)) \frac{\eta(z^\top z_1^-, \dots, z^\top z_k^-)}{\gamma(z, y)} \right] \right] \end{aligned} \quad (21)$$

$$\begin{aligned} &\geq \mathbb{E}_{(z,z^+,y) \sim p(z,z^+,y)} \left[\mathbb{E}_{z_{1:k}^- \sim \text{IID } r(\cdot | y)} \left[\psi(z^\top(z_1^- - z^+), \dots, z^\top(z_k^- - z^+)) \right] \cdot \frac{\mathbb{E}_{z_{1:k}^- \sim \text{IID } r(\cdot | y)} \left[\eta(z^\top z_1^-, \dots, z^\top z_k^-) \right]}{\gamma(z, y)} \right] \end{aligned} \quad (22)$$

$$\begin{aligned} &= \mathbb{E}_{(z,z^+,y) \sim p(z,z^+,y)} \left[\mathbb{E}_{z_{1:k}^- \sim \text{IID } r(\cdot | y)} \left[\psi(z^\top(z_1^- - z^+), \dots, z^\top(z_k^- - z^+)) \right] \right] \\ &= L_{SCL}(f) \end{aligned} \quad (23)$$

where (21) follows from (13) which defines $p_{HSC L}^-$, (22) follows from the application of the Harris inequality (see Lemma 1) to the inner expectation where z and z^+ are held fixed, and (23) follows from the definition of $\gamma(z, y)$ in (11). \square

A.2 Some details related to Theorem 2 and its proof

The following computations show that the zero mean and unit-norm conditions on the class means follow from the equal angle condition coupled with the fact that the representations $f(\cdot)$ are confined to lie within the unit-sphere in \mathbb{R}^{d_z} .

$$0 \leq \left\| \sum_{j \in \mathcal{Y}} \mu_y \right\|^2 = \sum_{j, \ell \in \mathcal{Y}} \mu_j^\top \mu_\ell = \sum_{j, \ell \in \mathcal{Y}, j \neq \ell} \underbrace{\mu_j^\top \mu_\ell}_{=\frac{-1}{C-1}} + \sum_{j \in \mathcal{Y}} \underbrace{\|\mu_j\|^2}_{\leq 1} \leq -\frac{C(C-1)}{C-1} + \sum_{j \in \mathcal{Y}} 1 = -C + C = 0.$$

Thus $\|\sum_{j \in \mathcal{Y}} \mu_y\|^2 = 0$ and for all $j \in \mathcal{Y}$, $\|\mu_j\|^2 = 1$.

Remark 2. We note that the lower bound of Theorem 2 also holds if we replace the unit-ball constraint on representations $\|z\| \leq 1$ with the weaker requirement $\frac{1}{C} \sum_{j=1}^C \|\mu_j\|^2 \leq 1$.

A.3 Proof of Theorem 3

Proof. The assumed distributional structure in the theorem statement corresponds to the setting in which there are C ‘‘latent clusters’’ labeled $y = 1, \dots, C$ and the positive and anchor samples in representation space, z, z^+ , are drawn from the same cluster y in an IID manner with distribution $s(\cdot|y)$ with the cluster y chosen uniformly at random. Each negative sample in representation space z_j^- is chosen independently of the anchor, positive, and all other negative samples by first choosing a cluster y_j^- uniformly at random and then sampling from the distribution $s(\cdot|y_j^-)$.

For $i = 1 : k$, we define the following indicator random variables $b_i := 1(y \neq y_i)$ and note that for all $i = 1 : k$, b_i is a deterministic function of (y, y_i^-) . Since $y \perp\!\!\!\perp \{y_{1:k}^-\}$ and $y_{1:k}^- \sim \text{IID Uniform}(\mathcal{Y})$, it follows that $b_{1:k} \sim \text{IID}$ and independent of y .

$$\begin{aligned} L_{UCL} &= \mathbb{E}[\psi(z^\top(z_1^- - z^+), \dots, z^\top(z_k^- - z^+))] \\ &\geq \mathbb{E}[\psi(\mathbb{E}[z^\top(z_1^- - z^+)|y, y_{1:k}^-], \dots, \mathbb{E}[z^\top(z_k^- - z^+)|y, y_{1:k}^-])] \end{aligned} \quad (24)$$

$$= \mathbb{E}[\psi(\mathbb{E}[z^\top(z_1^- - z^+)|y, y_1^-], \dots, \mathbb{E}[z^\top(z_k^- - z^+)|y, y_k^-])] \quad (25)$$

$$= \mathbb{E}[\psi(\mu_y^\top \mu_{y_1^-} - \|\mu_y\|^2, \dots, \mu_y^\top \mu_{y_k^-} - \|\mu_y\|^2)] \quad (26)$$

$$\geq \mathbb{E}[\psi(\mathbb{E}[\mu_y^\top \mu_{y_1^-} - \|\mu_y\|^2|b_{1:k}], \dots, \mathbb{E}[\mu_y^\top \mu_{y_k^-} - \|\mu_y\|^2|b_{1:k}])] \quad (27)$$

$$= \mathbb{E}[\psi(\mathbb{E}[\mu_y^\top \mu_{y_1^-} - \|\mu_y\|^2|b_1], \dots, \mathbb{E}[\mu_y^\top \mu_{y_k^-} - \|\mu_y\|^2|b_k])] \quad (28)$$

$$= \mathbb{E}[\psi(b_1 \mathbb{E}[\mu_y^\top \mu_{y_1^-} - \|\mu_y\|^2|b_1], \dots, b_k \mathbb{E}[\mu_y^\top \mu_{y_k^-} - \|\mu_y\|^2|b_k])] \quad (29)$$

$$= \mathbb{E}[\psi(b_1 \mathbb{E}[\mu_y^\top \mu_{y_1^-} - \|\mu_y\|^2|b_1 = 1], \dots, b_k \mathbb{E}[\mu_y^\top \mu_{y_k^-} - \|\mu_y\|^2|b_k = 1])] \quad (30)$$

$$= \mathbb{E}[\psi\left(\frac{b_1 \sum_{\ell \neq j} (\mu_j^\top \mu_\ell - \|\mu_j\|^2)}{C(C-1)}, \dots, \frac{b_k \sum_{\ell \neq j} (\mu_j^\top \mu_\ell - \|\mu_j\|^2)}{C(C-1)}\right)] \quad (31)$$

$$= \mathbb{E}[\psi\left(\frac{b_1 (\|\sum_j \mu_j\|^2 - C \sum_j \|\mu_j\|^2)}{C(C-1)}, \dots, \frac{b_k (\|\sum_j \mu_j\|^2 - C \sum_j \|\mu_j\|^2)}{C(C-1)}\right)] \quad (32)$$

$$\geq \mathbb{E}[\psi\left(\frac{b_1(0-C \cdot C)}{C(C-1)}, \dots, \frac{b_k(0-C \cdot C)}{C(C-1)}\right)] \quad (33)$$

$$= \mathbb{E}[\psi\left(\frac{-Cb_1}{(C-1)}, \dots, \frac{-Cb_k}{(C-1)}\right)]$$

$$= \frac{1}{C^{k+1}} \sum_{y, y_{1:k}^- \in \mathcal{Y}} \psi\left(\frac{-C1(y_1^- \neq y)}{(C-1)}, \dots, \frac{-C1(y_k^- \neq y)}{(C-1)}\right) \quad (34)$$

where the validity of each numbered step in the above sequence of inequalities is explained below.

Inequality (24) is Jensen’s inequality conditioned on $(y, y_{1:k})$ applied to the convex function ψ .

Equality (25) holds because for all $i \in \mathcal{Y}$, $\mathbb{E}[z^\top(z_i^- - z^+)|y, y_{1:k}] = \mathbb{E}[z^\top(z_i^- - z^+)|y, y_i]$ which is true because $\{y_\ell^-, \ell \neq i\} \perp\!\!\!\perp \{z, z^+, z_i^-\}$.

Equality (26) holds because $(z \perp\!\!\!\perp z^+)|y$, for all $i = 1 : k$, $(z \perp\!\!\!\perp z_i^-)|(y, y_i^-)$, and for all $i = 1 : k$ and all $j \in \mathcal{Y}$ we have $\mu_j = \mathbb{E}[z|y = j] = \mathbb{E}[z^+|y = j] = \mathbb{E}[z_i^-|y_i^- = j]$.

Inequality (27) is Jensen’s inequality conditioned on $b_{1:k}$ applied to the convex function ψ .

Equality (28) holds because for all $i = 1 : k$, $(y, y_i^-) \perp\!\!\!\perp \{b_\ell, \ell \neq i\}|b_i$.

Equality (29) holds because if $b_i = 0$, then $\mu_{y_i^-} = \mu_y$ and $\mu_y^\top \mu_{y_i^-} - \|\mu_y\|^2 = 0$.

Equality (30) holds because the expressions to the right of the equality symbols in (29) and (30) match when $b_i = 0$ and when $b_i = 1$.

Equality (31) holds because for each $i = 1 : k$, $y, y_i^- \sim \text{IID Uniform}(\mathcal{Y})$ and $y \neq y_i^-$ when $b_i = 1$.

Equality (32) follows from elementary linear algebraic operations.

Inequality (33) holds because ψ is argument-wise non-decreasing, the smallest possible value for $\|\sum_j \mu_j\|^2$ is zero and the largest possible value for $\|\mu_j\|$ is one.

Equality (33) follows from the definition of the indicator variables in terms of $y, y_{1:k}^-$ and because $y, y_{1:k}^-$ are IID Uniform(\mathcal{Y}).

Similarly to the proof of Theorem 2, if ψ is argument-wise *strictly* increasing, then equality holds in (33) iff for all $j \in \mathcal{Y}$, $\|\mu_j\| = 1$ (the unit-norm condition in Theorem 3) and $\sum_{j \in \mathcal{Y}} \mu_j = 0$ (the zero sum condition in Theorem 3).

Similarly to the proof of Theorem 2, if ψ is *strictly* convex, then equality in Jensen’s inequality (27) holds iff the equal angles condition in Theorem 3).

Finally, equality in (24) holds if it holds in (33) for reasons paralleling those for equality in (17) in the proof of Theorem 2. □

B ADDITIONAL EXPERIMENTS

We replicated the same experiments conducted in Sec. 5 on CIFAR10. The results are plotted in Fig. 3 and Fig. 4. In contrast to CIFAR10 and CIFAR100 where the numerical results are provided under three different settings, namely, unit-ball normalization with random initialization, unit-ball normalization with neural collapse initialization, and unit-sphere normalization with random initialization, for Tiny-ImageNet, we only conduct the experiment under unit-ball normalization with random initialization. This is because the size of Tiny-ImageNet (120000 images) is much larger than cifar (50000 images). Which results in a significantly longer processing time. The results for Tiny-ImageNet are plotted in Fig. 5.

B.1 Neural collapse and dimensional collapse

For CIFAR10, from Fig. 3 and Fig. 4, we observe similar phenomena as that for CIFAR100. Here again we note that while Theorems 2 and 3 suggest that neural collapse should occur in both the supervised and unsupervised scenarios when using the random negative sampling method, one may not be able to observe neural collapse in unsupervised settings. For the supervised case in CIFAR10, any degree of hardness propels the representation towards neural collapse. This may be due to the small number of classes in CIFAR10.

For Tiny-ImageNet, from Fig. 5, we observe that when $\beta = 5, 10, 30$, the geometry of the learned representation closely aligns with that of neural collapse. However, in HUCL, a high degree of hardness can be harmful. At $\beta = 5$, the geometry most closely approximates the neural collapse for both CIFAR10 and

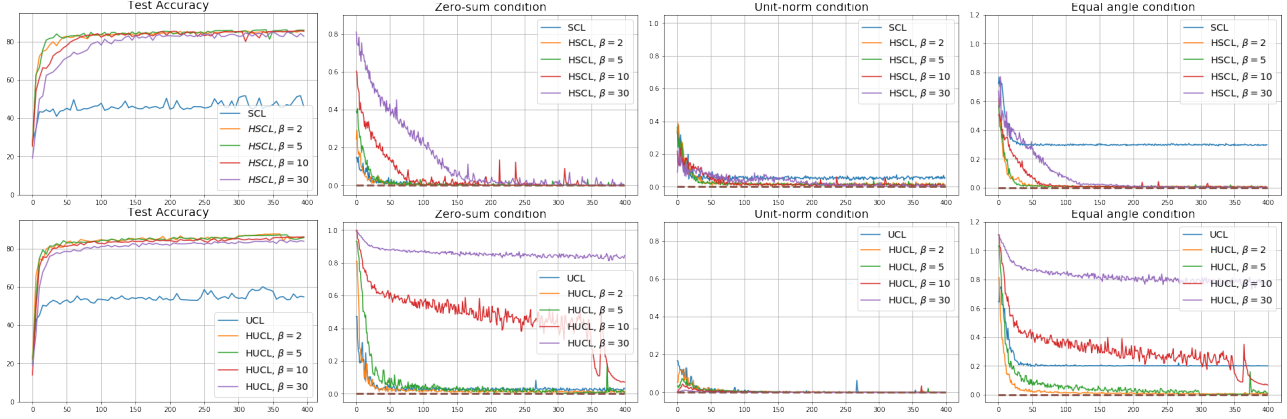


Figure 3: Results for CIFAR10 under supervised settings (SCL, HSCL, top row) and unsupervised settings (UCL, HUCL, bottom row) with unit-ball normalization and random initialization. From left to right: Downstream Test Accuracy, Zero-sum metric, Unit-norm metric, and Equal angle metric *vs.* number of Epochs.

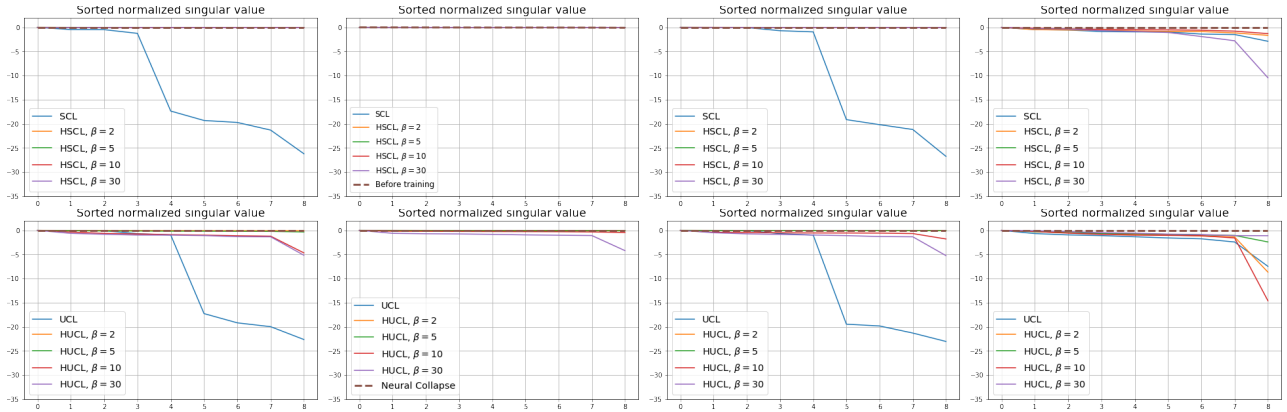


Figure 4: Normalized singular values of empirical covariance matrix of class means (in representation space) plotted in log-scale for CIFAR10 under supervised (top row) and unsupervised (bottom row) settings. From left to right: Unit-ball normalization with random initialization, Unit-ball normalization with NC initialization, Unit-sphere normalization with random initialization, and un-normalized representation with random initialization.

Tiny-ImageNet. However, increasing the degree of hardness further, for example at $\beta = 30$, causes the center of class means to deviate from the origin and also equal-angularity is heavily violated.

Furthermore, from the the normalized singular values for CIFAR10 in Fig. 4 and for Tiny-ImageNet in Fig. 5 we observe that random negative sampling suffers from DC while hard negative sampling consistently mitigates DC. The supervised case benefits more from a higher degree of hardness, since in the unsupervised cases there are higher chances of class collisions.

B.2 Role of initialization and normalization

As observed from Fig. 4 we note that the effect of initialization and normalization on the learned representation geometry is similar to that for CIFAR100.

Role of initialization: We note that 1) SCL and HSCL trained with near-NC initialization and ADAM do

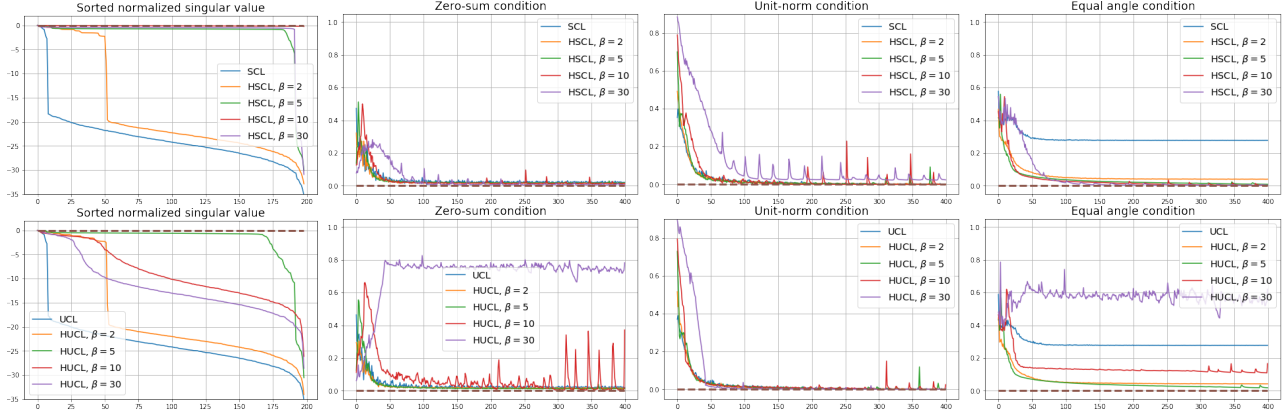


Figure 5: Results for Tiny-ImageNet under supervised settings (SCL, HSCL, top row) and unsupervised settings (UCL, HUCL, bottom row) with unit-ball normalization and random initialization. From left to right: Sorted normalized singular values in last epoch, Zero-sum metric, Unit-norm metric, and Equal angle metric *vs.* number of Epochs.

not exhibit DC and 2) UCL trained with near-NC initialization and ADAM also does not exhibit DC, but the behavior of HUCL depends on the hardness level β .

Role of normalization: As observed, the behavior of unit-sphere normalization is close to that of unit-ball normalization, and with hard negative sampling, both SCL and UCL can achieve NC. Without normalization, neither regular nor hard negative training methods attain NC and they suffer from DC. We also observe that with regular negative sampling, un-normalized representations leads to a lower degree of DC for both SCL and UCL. However, hard-negative sampling benefits more from feature normalization and its absence leads to more severe DC. The phenomenon of DC is not as obvious as the one in CIFAR100, which may be because CIFAR10 has only 10 classes.

Algorithm 1 Contrastive Learning Algorithm

Require: Batch size N , data \mathcal{X} , label \mathcal{Y} , neural-net parameters of representation function f , Algorithm:

SCL/ UCL/HSCL/HUCL, normalization type: unit-ball/unit-sphere/no-normalization, hardening function

$$\eta(t_{1:k}) := \prod_{i=1}^k e^{\beta t_i}, \beta > 0.$$

- 1: Define negative distribution $p^-(z_{1:k}^- | z, z^+)$ based on the chosen Algorithm, see section 3 for details.
 - 2: **for** each sampled minibatch $\{x_i\}_{i=1}^N$ **do**
 - 3: **for** all $i \in \{1, \dots, N\}$ **do**
 - 4: Compute $f(x_i)$
 - 5: **if** unit-ball normalization **then**
 - 6: **if** $\|f(x_i)\| \leq 1$ **then**
 - 7: $z_i = f(x_i)$
 - 8: **else**
 - 9: $z_i = \frac{f(x_i)}{\|f(x_i)\|}$
 - 10: **end if**
 - 11: **else if** unit-sphere normalization **then**
 - 12: $z_i = \frac{f(x_i)}{\|f(x_i)\|}$
 - 13: **else if** no-normalization **then**
 - 14: $z_i = \frac{f(x_i)}{\sqrt{d}}$
 - 15: **end if**
 - 16: **end for**
 - 17: **for** all $i \in \{1, \dots, N\}$ **do**
 - 18: **for** all $j \in \{1, \dots, N\}$ **do**
 - 19: **if** $y(x_i) = y(x_j)$ **then**
 - 20: Draw $\{z_{1:k}^-\}$ from $p^-(z_{1:k}^- | z_i, z_j)$
 - 21: $\{v_{i,j,m}\}_{m=1}^k = \{z_i^\top z_m^- - z_i^\top z_j\}_{m=1}^k$
 - 22: $\ell_{i,j} = \log \left(1 + \frac{1}{k} \sum_{m=1}^k e^{v_{i,j,m}} \right)$
 - 23: **else**
 - 24: $\ell_{i,j} = 0$
 - 25: **end if**
 - 26: **end for**
 - 27: **end for**
 - 28: Compute the average loss: $L = \frac{1}{|\{\ell_{ij} \neq 0\}|} \sum_{i=1}^N \sum_{j=1}^N \ell_{i,j}$
 - 29: Take one stochastic gradient step using ADAM
 - 30: **end for**
 - 31: **return** Encoder network $f(\cdot)$
-